






Noninvasive Mapping of Ripple Onset Predicts Outcome in Epilepsy Surgery

Eleonora Tamilya, PhD ^{1,2} Margherita A. G. Matarrese, MSc ^{1,3}
Georgios Ntolkeras, MD ^{1,2} P. Ellen Grant, MD,² Joseph R. Madsen, MD,⁴
Steve M. Stuffelbeam, MD,⁵ Phillip L. Pearl, MD ⁶ and
Christos Papadelis, PhD ^{1,7,8,9}

Objective: Intracranial electroencephalographic (icEEG) studies show that interictal ripples propagate across the brain of children with medically refractory epilepsy (MRE), and the onset of this propagation (ripple onset zone [ROZ]) estimates the epileptogenic zone. It is still unknown whether we can map this propagation noninvasively. The goal of this study is to map ripples (ripple zone [RZ]) and their propagation onset (ROZ) using high-density EEG (HD-EEG) and magnetoencephalography (MEG), and to estimate their prognostic value in pediatric epilepsy surgery.

Methods: We retrospectively analyzed simultaneous HD-EEG and MEG data from 28 children with MRE who underwent icEEG and epilepsy surgery. Using electric and magnetic source imaging, we estimated virtual sensors (VSs) at brain locations that matched the icEEG implantation. We detected ripples on VSs, defined the virtual RZ and virtual ROZ, and estimated their distance from icEEG. We assessed the predictive value of resecting virtual RZ and virtual ROZ for postsurgical outcome. Interictal spike localization on HD-EEG and MEG was also performed and compared with ripples.

Results: We mapped ripple propagation in all patients with HD-EEG and in 27 (96%) patients with MEG. The distance from icEEG did not differ between HD-EEG and MEG when mapping the RZ (26–27mm, $p = 0.6$) or ROZ (22–24mm, $p = 0.4$). Resecting the virtual ROZ, but not virtual RZ or the sources of spikes, was associated with good outcome for HD-EEG ($p = 0.016$) and MEG ($p = 0.047$).

Interpretation: HD-EEG and MEG can map interictal ripples and their propagation onset (virtual ROZ). Noninvasively mapping the ripple onset may augment epilepsy surgery planning and improve surgical outcome of children with MRE.

ANN NEUROL 2021;89:911–925

Epilepsy surgery is the therapy of choice for children with medically refractory epilepsy (MRE). The goal of epilepsy surgery is to resect the epileptogenic zone (EZ), the brain area indispensable for the generation of seizures.¹ However, identifying this zone is challenging.^{2,3} In ~25% of patients, noninvasive techniques cannot formulate a clear hypothesis regarding the EZ.^{2,4} For them,

an invasive evaluation is recommended, which consists of long-term intracranial electroencephalography (icEEG) with macroelectrodes directly implanted into or onto the brain. The main purpose of icEEG is to record seizures and trace the seizure onset zone (SOZ), the most logical EZ estimator.¹ Nonetheless, seizures are unpredictable; their recording can be time-consuming and come at the

View this article online at [wileyonlinelibrary.com](https://www.wileyonlinelibrary.com). DOI: 10.1002/ana.26066

Received Sep 28, 2020, and in revised form Mar 9, 2021. Accepted for publication Mar 10, 2021.

Address correspondence to Dr Papadelis, Jane and John Justin Neurosciences Center, Cook Children's Health Care System, 1500 Cooper St, Fort Worth, TX 76104. E-mail: christos.papadelis@cookchildrens.org

From the ¹Laboratory of Children's Brain Dynamics, Division of Newborn Medicine, Department of Medicine, Boston Children's Hospital, Harvard Medical School, Boston, MA; ²Fetal-Neonatal Neuroimaging and Developmental Science Center, Boston Children's Hospital, Harvard Medical School, Boston, MA; ³Laboratory of Nonlinear Physics and Mathematical Modeling, Department of Engineering, University Bio-Medico Campus of Rome, Rome, Italy; ⁴Epilepsy Surgery Program, Department of Neurosurgery, Boston Children's Hospital, Harvard Medical School, Boston, MA; ⁵Athinoula A. Martinos Center for Biomedical Imaging, Massachusetts General Hospital, Harvard Medical School, Boston, MA; ⁶Division of Epilepsy and Clinical Neurophysiology, Department of Neurology, Boston Children's Hospital, Harvard Medical School, Boston, MA; ⁷Jane and John Justin Neurosciences Center, Cook Children's Health Care System, Fort Worth, TX; ⁸School of Medicine, Texas Christian University and University of North Texas Health Science Center, Fort Worth, TX; and ⁹Department of Bioengineering, University of Texas at Arlington, Arlington, TX

expense of substantial resources. The availability of interictal biomarkers that estimate the EZ noninvasively without the need to wait for unpredictable seizures is paramount.

Several studies investigated interictal high-frequency oscillations (HFOs) as an alternative to seizures.^{5–9} HFOs are recorded both invasively with icEEG and noninvasively with EEG and/or magnetoencephalography (MEG).^{7,10,11} HFOs are classified into ripples (>80Hz) and fast ripples (>250Hz).⁵ Fast ripples are closely linked to epileptogenicity but can be too focal to be captured with conventional icEEG^{6,12,13} and difficult to detect noninvasively. In contrast, ripples can be recorded with conventional icEEG and detected using EEG and MEG, although less frequently.^{14–18} Nonetheless, the presurgical value of ripples has been long debated, because they are seen over large areas (called ripple zones [RZs]),^{12,19,20} which may also encompass nonepileptogenic regions that generate physiological ripples.

Two research groups independently showed that ripples propagate across icEEG electrodes in patients with MRE,^{21,22} and the onset of this propagation (ripple onset zone [ROZ]) is more predictive of surgical outcome compared to areas of spread.²¹ This prompts the value of mapping ripples before surgery and raises the question of whether noninvasive techniques can map this propagation and identify the ROZ. Using MEG and high-density EEG (HD-EEG), virtual sensors (VSs) can be reconstructed at desired brain locations to increase the signal-to-noise ratio (SNR), facilitating the noninvasive identification of ripples.^{23–28} Nonetheless, it remains unknown whether a noninvasive implantation of VSs can capture the propagation phenomenon and define an epilepsy biomarker (the ROZ) that so far is known exclusively on invasive icEEG, which currently constitutes the technique of choice for recording ripples and their propagation. Such a virtual implantation could potentially augment presurgical planning and outcomes of epilepsy surgery.

Here, we aim to map noninvasively the spatiotemporal propagation of interictal ripples across the brain of children with MRE using a virtual implantation and to assess the prognostic value of resecting the noninvasively localized areas that initiate this propagation. We hypothesize that areas that initiate the ripple propagation can be identified noninvasively and their proximity to resection predicts outcome. To test our hypothesis, we reconstructed VSs in children with MRE, detected ripples and their onset on VSs, and compared them with the icEEG-defined RZ and ROZ as well as with resection and outcome. VSs were placed to match the icEEG location to enable direct comparison between

the proposed noninvasive approach and the invasive benchmark.^{21,22}

Patients and Methods

Patients

We retrospectively reviewed patients with MRE who underwent epilepsy surgery at Boston Children's Hospital (BCH) between June 2011 and June 2018. We included patients with (1) preoperative HD-EEG and MEG, (2) long-term icEEG, (3) ≥ 1 -year follow-up, (4) postimplantation computerized tomography (CT), and (5) preoperative and postoperative magnetic resonance imaging (MRI). Patients were excluded if < 5 minutes of good-quality high-frequency data (≥ 80 Hz) were available for HD-EEG or MEG.¹⁵ The study protocol received approval by the institutional review board of BCH (IRB-P00022114), which waived the need for informed consent due to the retrospective nature.

Simultaneous HD-EEG/MEG Recordings

HD-EEG/MEG recordings were conducted at the MEG Laboratory of Athinoula Martinos Center for Biomedical Imaging (Charlestown, MA) in a 3-layer magnetically shielded room (Imedco, Hägendorf, Switzerland) with a whole-head 306-channel MEG system (Neuromag VectorView, Elekta, Helsinki, Finland). HD-EEG was recorded with 70-channel electrode caps (EASYCAP, Herrsching, Germany) plus 2 temporal electrodes (T1/T2). More details about the protocol can be found in previous studies.^{15,17,29} Data were recorded for 10 to 12 sessions (4 minutes each; sampling rate: 600, 1000, or 2000Hz). We analyzed sessions regarded as containing interictal activity by the attending epileptologist regardless of the patient's vigilance state.¹⁵ Data quality was checked using standard (1–70Hz, 10 s/page) and HFO display settings (80–200Hz, 4 s/page). Segments were regarded as good quality in the high-frequency range when showing regular low-amplitude background with HFO display settings. Given the low SNR of scalp EEG and MEG signals for frequencies greater than 200Hz, no fast ripples were considered, and ripples were limited to frequencies less than 200Hz. Finally, we selected epochs free of artifacts, high-frequency noise, and technical disruptions.

icEEG Recordings

icEEG was recorded with subdural (10mm distance) and/or depth electrodes (3–5mm interdistance; Ad-Tech, Racine, WI) using XLTEK NeuroWorks (Natus, Pleasanton, CA). Per our institution's clinical practice, pediatric epileptologists reviewed each patient's icEEG daily and extracted multiple 5- to 10-minute segments containing interictal epileptiform activity. We retrospectively reviewed these segments and

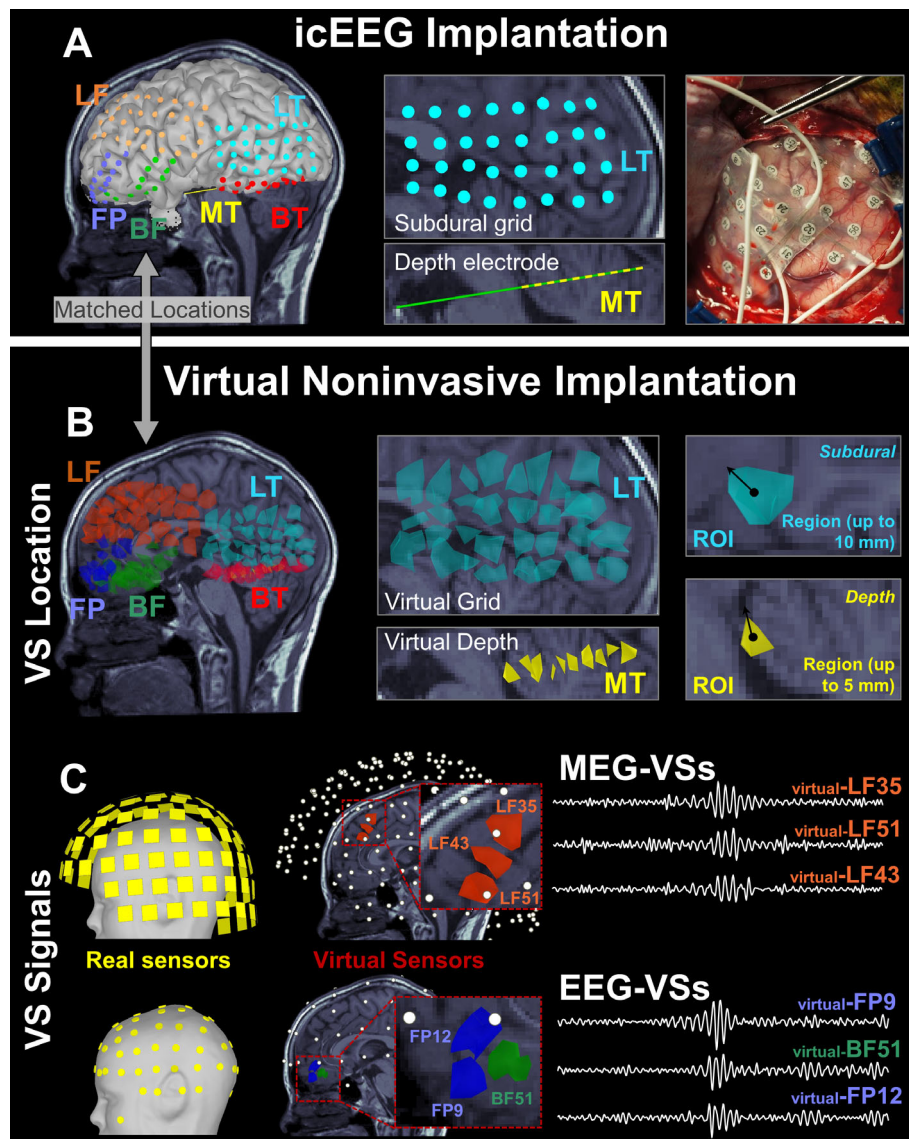


FIGURE 1: Virtual sensor (VS) implantation using magnetoencephalography (MEG) and high-density electroencephalographic (EEG) data. (A) Example of intracranial EEG (icEEG) implantation with both subdural and depth electrodes on the left temporal (LT) and medial temporal (MT) lobe of a 12-year-old boy (Patient 16). (B) Placement of VSs (or regions of interest [ROIs]) based on the coordinates of icEEG electrodes (matched locations). Nonoverlapping ROIs were defined for each electrode in the patient's source space as the volume points showing a distance from the electrode center below threshold (ie, 10mm for subdural and 5mm for depth electrodes). Such a threshold for the ROI definition was set based on the interelectrode distance. (C) Reconstruction of VS signal (time series): mean activity of each ROI (or VS) across time, reconstructed based on the data recorded by the actual MEG or EEG sensors. BF = basal frontal; BT = basal temporal; FP = frontal pole; LF = left frontal.

selected 5 to 10 minutes of data. This duration was shown to be robust to possible HFO propagation changes across time.²¹ Channels with continuous artifacts were excluded.

The location of icEEG contacts was determined on patients' presurgical MRI coregistered with postimplantation CT (Fig 1A) using Brainstorm.³⁰ To account for brain shift that occurs after electrocorticographic implantation,³¹ subdural electrodes were projected onto the cortical surface (reconstructed via FreeSurfer). When both subdural and depth electrodes were implanted, depth electrodes were also adjusted to compensate for brain shift.³¹

VS Reconstruction

VSs were placed to match the icEEG contacts (see Fig 1B). VS time series were reconstructed for HD-EEG and MEG separately (see Fig 1C).

Beamformer Analysis.

We extracted cortical surfaces from the preoperative MRIs via FreeSurfer³² and constructed realistic head models using OpenMEEG³³ (3-layer boundary elementary model).^{15,29} Source space included the entire brain volume.

We used linearly constrained minimum variance beamformer, implemented in Brainstorm, to estimate brain activity within the source space. Data covariance was computed from 200-millisecond windows around each spike, filtered between 80 and 200Hz.²⁶ For noise covariance, we used 10 seconds of broadband data (1–300Hz) without epileptiform activity. A source activation map (covering all volume points) was generated for each time point.

Virtual Sensors. Beamformer output was used to reconstruct the activity of selected brain locations (VSs), where the icEEG electrodes had been implanted during the patient's phase 2 evaluation. For each icEEG electrode, we delineated nonoverlapping regions of interest that included the closest volume points surrounding the electrode's center, up to 5 or 10mm for depth or subdural electrode, respectively (see Fig 1B). Finally, we reconstructed each VS's time series by computing its mean activation (mean across volume points) for HD-EEG and MEG separately (see Fig 1C).

Ripple Detection

Automated ripple detection²¹ was performed on icEEG and VSs. Given the low SNR of HD-EEG and MEG signals greater than 200Hz, detection on VSs was performed between 80 and 200Hz using an envelope threshold of 4 standard deviations (SDs), which is lower than on icEEG (5 SDs).²¹ The detector identifies as ripples only events showing an "island" in the time–frequency plane (Fig 2).²¹ We analyzed ripples independently from other features (eg, overlap with spikes, amplitude, or morphology) that may discriminate pathological from physiological events, because no well-established methods exist to this purpose, particularly for scalp EEG/MEG. In addition, the importance of ripple propagation in MRE is only known from icEEG studies, where all ripples were considered, independently from other features.^{21,22}

We computed ripple rates for each icEEG electrode (ripples/min) and normalized them with respect to their maximum per patient.²¹ Similarly, we computed normalized ripple rates for VSs (HD-EEG and MEG separately), which we will refer to as "virtual ripple rate."

Spatiotemporal Propagation of Ripples

To characterize the spatiotemporal propagation of ripples and identify the ROZ (see Fig 2), we followed our previously described methodology,²¹ which automatically (1) finds propagation sequences, defined as at least 3 temporally overlapping ripples in neighboring contacts (<30mm apart); and (2) detects onset ripples of each

sequence (occurring within 10 milliseconds from propagation onset).

For each patient, we computed the rate of onset ripples of each icEEG electrode and normalized it. Similarly, we computed normalized rates of onset ripples per VS (for HD-EEG and MEG separately), which we call "virtual onset ripple rate." The icEEG electrodes with a normalized rate of onset ripples greater than 0.8²¹ defined the intracranial ROZ as the brain tissue within 10mm from their center (Fig 3A, red volume). Similarly, intracranial RZ was defined by icEEG electrodes with a normalized ripple rate greater than 0.8 (independently from propagation analysis).

Comparison with icEEG

We assessed the ability of VSs to localize RZ or ROZ by comparing the location of VSs showing ripples or onset ripples with the icEEG-defined ripple zones. We quantified the performance of the virtual ripple rate to identify the VSs within the intracranial RZ (see Fig 3A) by estimating the area under the curve (AUC) of the receiver operating characteristic (ROC) curves (built for each patient and modality). Similarly, we built ROC curves on the virtual onset ripple rate to assess its ability to localize the intracranial ROZ. We averaged ROC curves for RZ and ROZ separately and identified the optimal operating point (through Youden index). VSs were regarded as belonging to RZ or ROZ when their rate was above the optimal cutoff. The median distance of these VSs from the icEEG-defined RZ or ROZ (D_{icEEG}) was calculated per patient (see Fig 3A) separately for HD-EEG and MEG.

Resection and Postsurgical Outcome

We coregistered preoperative and postoperative MRIs using Brainstorm and defined the resection volume (see Fig 3B, C). For each VS, we calculated their distance from resection (D_{RES}) as the Euclidean distance of their center from the closest resection margin (see Fig 3B, C).³⁴ VSs were considered resected when D_{RES} was ≤ 10 mm. Considering a mean gyral width of 11 to 21mm,^{35,36} we defined concordance, across the whole study, as a 10mm distance or less (which can be interpreted as a measure of gyral-width concordance).

Postsurgical outcome was evaluated using Engel classification based on the most recent follow-up at least 12 months after surgery and dichotomized into good (Engel IA–D) and poor (Engel class \geq II).

Outcome Prediction

To test whether the virtual mapping of RZ and ROZ helps surgical planning, we evaluated whether this could classify the tissue around each VS as epileptogenic or not.

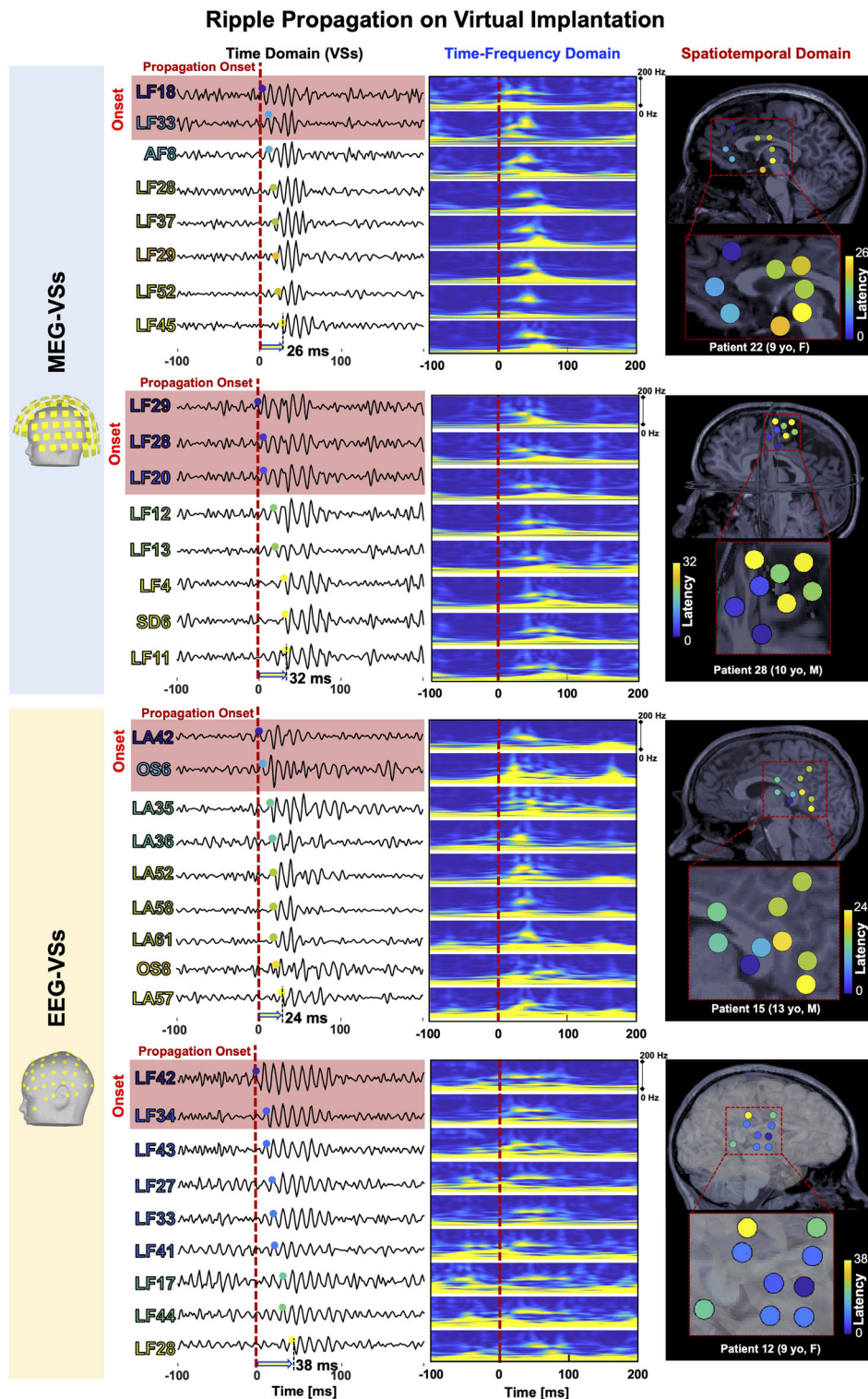


FIGURE 2: Ripple propagation on virtual sensors (VSs). Examples are shown of ripple propagation on magnetoencephalography (MEG) VSs (top) and electroencephalographic (EEG) VSs (bottom). Each scenario shows the ripple propagation in (1) the time domain (left), where ripples are seen on adjacent VSs with a certain temporal latency from the onset (red dashed line; VSs showing onset ripples, ie, within 10 milliseconds from the onset, are highlighted in blue); (2) the time–frequency domain (middle), where ripples are seen as an island in the spectral content within the ripple frequency band (80–200Hz); and (3) the spatiotemporal domain (right), where the VSs involved in the propagation are displayed on the patient’s magnetic resonance imaging and color coded by their temporal latency from the onset. F = female; M = male; yo = years old.

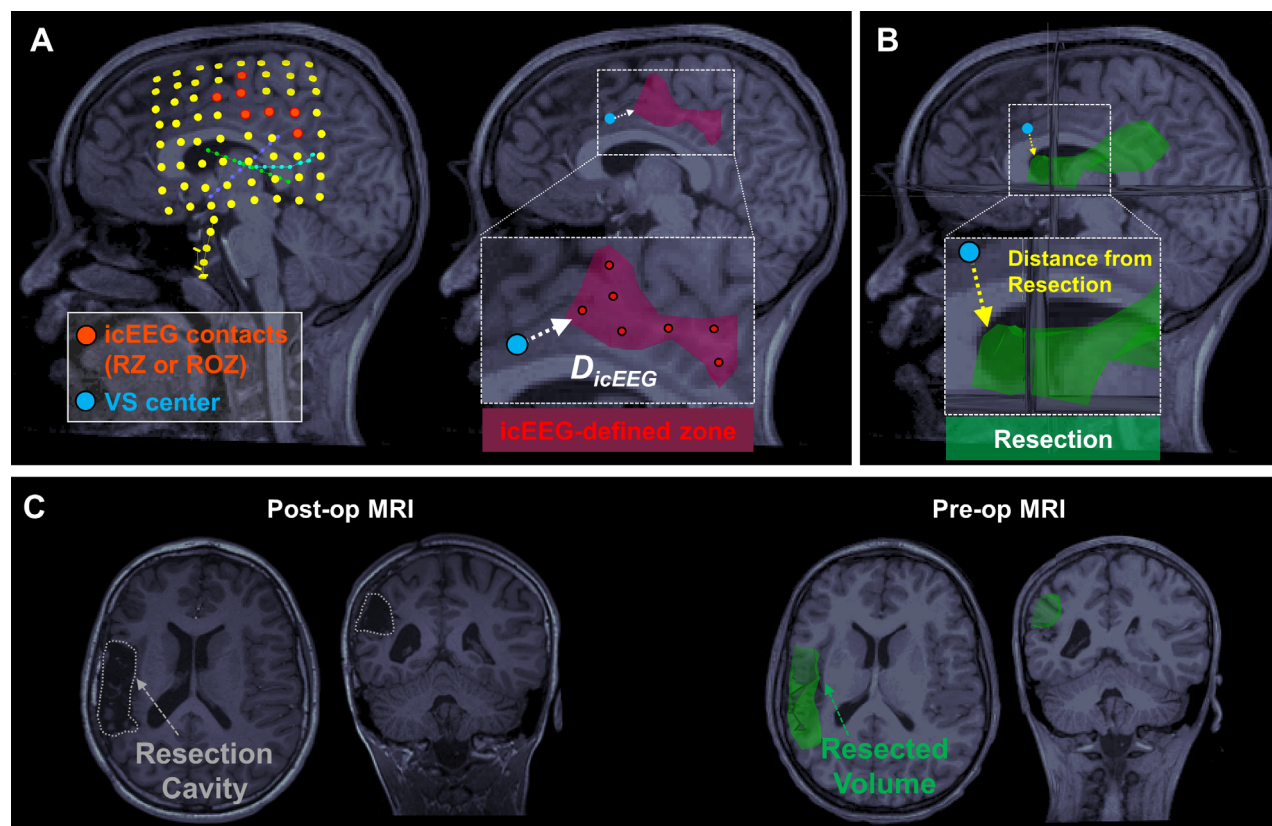


FIGURE 3: Comparison of virtual sensor (VS) estimates with invasive electroencephalography (EEG) and resection. (A) Left: Localization of intracranial EEG (icEEG) contacts on a patient's preoperative magnetic resonance imaging (MRI) after coregistration with postimplantation computed tomography. icEEG contacts recording high rates of ripples (or onset ripples) are marked in red. Right: Brain tissue surrounding the high-rate icEEG contacts (up to 10mm from their center) defines the invasive benchmark (red volume). D_{icEEG} is estimated as the distance between the VSs (light blue) recording a high rate of ripples (or onset ripples) and the icEEG-defined ripple zones (RZs; white arrow). (B,C) The resected volume (in green) was marked on the preoperative MRI after coregistration with postoperative MRI, where the resection cavity was identifiable. The distance of a VS from the resection was computed as its Euclidean distance from the closet margin of the resected volume (yellow arrow). ROZ = ripple onset zone.

For each patient, we defined virtual RZ or virtual ROZ by identifying the VS(s) with high rates of ripples or onset ripples. The optimal threshold to identify these VSs was not known a priori. Thus, we varied the threshold from 0 to 100% of the patient's maximum rate (5% steps).²¹ The resection percentage of the obtained virtual zone was computed as the percentage of its VSs that were resected. We considered a zone to be resected when most of it was surgically removed (resection percentage > 50%).²¹ Good outcome following resection was regarded as true positive (TP) prediction and poor outcome following missed resection as true negative (TN) prediction. After estimating positive predictive value ($PPV = TP/[TP + \text{false positive (FP)}]$), negative predictive value ($NPV = TN/[TN + \text{false negative (FN)}]$), and prediction accuracy ($[(TP + TN)/(TP + TN + FP + FN)]$) for all thresholds, virtual RZ and virtual ROZ were defined as those providing the highest predictive performance. Median D_{RES} of virtual RZ and virtual ROZ were computed per patient.

Spike Localization and SOZ

We compared virtual ripple zones with the localization of spikes (which are the standard approach in HD-EEG/MEG source localization for epilepsy) and the icEEG-defined SOZ.

Spikes were identified by an experienced reader (C.P.) on HD-EEG and MEG independently.²⁹ Each individual spike was localized using an equivalent current dipole (as is common practice for HD-EEG/MEG at our institution) following the same methodology described in our previous study.²⁹ Spike average was not applied to avoid merging discharges with similar scalp topography albeit generated by different sources.³⁷ Dipoles with a goodness of fit less than 60% were discarded.²⁹

For each dipole, we estimated D_{RES} as well as distance from virtual RZ and virtual ROZ (as distance from the center of their closest VS), regarding them as overlapping when closer than 10mm. For each patient, we estimated the overall overlap (as percentage) with virtual

RZ, virtual ROZ, and resection. Finally, we automatically identified dipole clusters as groups of at least 5 dipoles³⁸ within 10mm distance and identified the anatomical location (frontal, central, parietal, temporal, occipital) of the preponderant cluster.

SOZ was defined by the contact(s) showing the earliest change associated with clinical seizures during icEEG monitoring (independently from this study). We calculated the distance of each VS from SOZ (D_{SOZ}), regarding them as overlapping when ≤ 10 mm apart.

Statistical Analysis

Wilcoxon signed rank test was used for paired comparisons between modalities and Wilcoxon rank sum for nonpaired comparisons between outcome groups. Nonparametric tests were used because variables were not normally distributed as established by Kolmogorov–Smirnov test. Fisher exact test was used to test association between resection of virtual RZ, virtual ROZ, or dipoles and outcome. *Phi* coefficient (−1 to 1) was estimated as a measure of association strength.

We considered $p \leq 0.05$ to be significant. Results are reported as median (interquartile range). MATLAB R2018a (MathWorks, Natick, MA) was used for statistics.

Results

Patient Cohort

Twenty-eight children with MRE (age at surgery = 12.5 [9–16] years) were included. Thirty-six patients met the inclusion criteria; 8 were excluded because of high-frequency noise (>80 Hz) on HD-EEG or MEG. Table 1 summarizes patients' characteristics. For icEEG, we analyzed 5.2 (5.0–6.3) minutes and 100 (87–121) contacts per patient without difference between outcomes ($p = 0.2$). Subdural electrodes were implanted in 11 patients, depth electrodes in 6 patients, and both types in 11 patients, with a total of 72% of contacts in the gray matter. For HD-EEG and MEG, we analyzed an average of 9.6 and 11 minutes of artifact-free data per patient. Average interval between HD-EEG/MEG and icEEG recordings was 6 (3–13) months.

Seventeen patients (61%) had good postsurgical outcome. An average of 1.26% (0.9–1.88%) of the brain was resected in our cohort without difference between outcomes ($p = 0.08$; see Tables 1 and 2). No differences were seen in sex, age at surgery and epilepsy onset, follow-up period, and pathology between outcomes (see Table 2).

Comparison with icEEG

Ripple Occurrence and Spatiotemporal Propagation. Ripples on VSs (HD-EEG and MEG) were detected in all patients. Ripple rates were lower on VSs than icEEG

($p < 0.001$), with EEG VSs recording higher rates than MEG VS (0.9 vs 0.4 ripples/min, $p < 0.001$; Table 3). Ripple propagation was observed in all patients using icEEG and EEG VSs, and in 27 patients (96%) using MEG VSs. Table 3 reports the spatiotemporal characteristics of propagation per modality. We detected more ripple propagations on icEEG than EEG VSs and MEG VSs (15 vs 5.4 vs 2.4 propagations/min, $p < 0.001$). Peak frequency of icEEG ripples was positively correlated with their amplitude ($p < 0.001$, $R = 0.2$); because MEG and HD-EEG are more sensitive to high-amplitude than low-amplitude ripples, this correlation may explain the slightly higher frequencies on VSs.

The propagation spatial extent was the longest on EEG VSs (41mm or 6 sensors per propagation) followed by MEG VSs and icEEG (32 and 36mm or 5 sensors; see Table 3). Temporal extent was longer on icEEG than VSs for both HD-EEG and MEG (86 vs 27 vs 22 milliseconds; see Table 3). Propagation onsets encompassed more channels when recorded by VSs than icEEG: 4 VSs per sequence for HD-EEG and MEG compared to 1 electrode for icEEG.

RZ and ROZ. ROC curve analysis showed that virtual ripple rate was able to identify the icEEG-defined RZ with median AUC of 0.76 (0.57–0.79) and 0.65 (0.54–0.79) for HD-EEG and MEG, respectively ($p = 0.24$; Fig 4A). AUC for HD-EEG and MEG was greater than 0.5 in 86% and 89% of our cohort, respectively. D_{icEEG} of the RZ defined by VSs did not differ between HD-EEG and MEG ($p = 0.6$, 27 vs 26mm; see Fig 4A), nor did their sensitivity (HD-EEG, 71% [9–100]; MEG, 50% [0–100]; $p = 0.67$) or specificity to the icEEG RZ (HD-EEG, 63% [51–81]; MEG, 69% [50–78]; $p = 0.77$).

Virtual onset ripple rate showed an AUC of 0.70 (0.35–0.85) and 0.64 (0.45–0.84) for HD-EEG and MEG, respectively ($p = 0.8$; see Fig 4B). AUC for HD-EEG and MEG was greater than 0.5 in 68% and 61% of our cohort. D_{icEEG} of the ROZ defined by the VSs did not differ between HD-EEG and MEG ($p = 0.4$, 24 and 22mm; see Fig 4B), nor did their sensitivity (HD-EEG, 61% [0–100]; MEG, 100% [0–100]; $p = 0.85$) or specificity to the icEEG ROZ (HD-EEG, 76% [58–87]; MEG, 70% [53–81]; $p = 0.19$). Average extent of VSs with high ripple rate and onset ripple rate was 11.3 and 6.3cm, respectively, when estimated via HD-EEG, and 7 and 5.3cm via MEG.

Overlap with Resection and Outcome

The virtual ROZ estimated via EEG VSs was closer to resection in good than in poor outcomes ($p = 0.0026$, $D_{RES} = 8$ vs 18mm); this was not found for the virtual RZ (see

TABLE 1. Patients' Demographics and Clinical Characteristics

#/Sex	Epilepsy			MRI Findings	icEEG Type (contacts, n)	icEEG Location	Spike Clusters,		Res Res Lobe Vol, %	Engel (f/u, mo)
	Age, yr	Onset, yr	Side				HD-EEG/ MEG, n ^a			
1/M	10	4	R	Normal	SE (80)	Fr, T	1/1	Fr	1.2	IA (44)
2/F	7	3	L	FCD (T and Ins)	DE (90)	T, lower Fr	Scattered	Fr/T	1.2	I (14)
3/F	9	0.3	L	Hippocampal sclerosis(mesial T, periventricular)	DE (140)	T, O, P	Scattered/1	T	1.2	IV (13)
4/F	13	10	L	Normal	SE (72)	T, Fr	1/1	T	1.5	IA (48)
5/M	17	9	L	Tumor (T)	SE + DE (92)	T, Fr	2/2	T	2.7	ID (13)
6/M	2	0.33	R	TSC (multifocal)	SE (112)	Fr, P, IE	Scattered/1	Fr	6.4	IB (41)
7/F	8	4	R	FCD (P)	SE + DE (100)	P O, IE	1/2	P	1.8	IB (43)
8/M	18	8	L	FCD (mesial T, periventricular)	SE (64)	T	Scattered	T	1.9	IA (26)
9/F	18	15	L	Normal	SE (88)	T, sub-Fr	Scattered/2	T	1.8	IA (29)
10/M	15	4	L	Normal	SE (88)	Fr, T, O	3/2	T	1.2	IIB (25)
11/M	16	4	L	Normal (mild gliosis)	SE (88)	T, P, post Fr	2/1	Fr	0.5	III (36)
12/F	9	1	R	Low-grade neoplasm (Fr)	SE + DE (122)	Fr, P, IE	1/scattered	Fr	1.3	IB (42)
13/F	18	4	L	FCD (Fr)	SE + DE (154)	Fr, P	Scattered	Fr	0.8	IIA (14)
14/F	14	6	L	FCD (mesial P)	SE (72)	Fr, P, T	1/1	P	0.9	IA (12)
15/M	13	8	L	Encephalomalacia (P, superior T)	SE + DE (102)	Fr, P, T	1/1	P-T	1.6	IIA (6)
16/M	12	7	L	FCD (T)	SE + DE (122)	Fr, T	Scattered	Fr-T	4.4	IIA (13)
17/M	13	0	L	Infarct (MCA territory)	SE (136)	Fr, T, P O	1/1	Fr-T	3.7	II (37)
18/M	22	5	L	FCD (C P)	SE + DE (94)	Fr	1/scattered	Fr	1.3	IA (17)
19/M	11	1	L	FCD (mesial T)	SE (92)	Fr, T	Scattered	T	2.9	IA (46)
20/M	16	5	L	FCD	DE (212)	Fr, T	1/1	Ins	0.5	III (24)
21/M	10	7	L	Polymicrogyria (Fr, P)	SE + DE (124)	Fr, T, ant P	1/1	Fr	3.3	IB (10)
22/F	9	8	L	FCD (Fr)	SE (96)	Fr, T, P	1/1	Fr P	0.4	III (25)
23/F	7	4	R	FCD (Fr operculum)	SE + DE (112)	Fr, T	1/1	Fr	1.2	II (31)
24/F	15	3	L	None	DE (212)	Fr, T, ant P	1/scattered	Fr	1.6	IA (27)
25/F	7	6	L	FCD (posterior Fr)	DE (164)	Fr, P, T	Scattered	Ins	1.2	IA (15)
26/F	18	3	L	FCD (Fr)	SE + DE (112)	Fr, ant T	1/1	Fr	0.6	IA (21)
27/F	4	0.5	R	None	DE (162)	Fr	Scattered/1	Ins	0.7	IA (12)
28/M	10	5	L	None	SE + DE (106)	P, post Fr	1/1	Fr	0.9	III (12)

^aSpike source localization: lobe containing main dipole cluster.

ant = anterior; CP = central; DE = depth electrodes; EEG = electroencephalography; F = female; f/u = follow-up; FCD = focal cortical dysplasia; Fr = frontal; HD = high-density; icEEG = intracranial EEG; IE = interhemispheric; Ins = insula; L = center; M = male; MCA = middle cerebral artery; MEG = magnetoencephalography; MRI = magnetic resonance imaging; O = occipital; P = parietal; post = posterior; R = right; Res = resection; SE = subdural electrodes; T = temporal; TSC = tuberous sclerosis complex; Vol = volume.

TABLE 2. Patients' Demographics by Outcome

Characteristic	Total	Good Outcome, Engel I	Poor Outcome, Engel II–IV	<i>p</i>
n	28	17	11	
M/F, n	14/14	7/10	7/4	0.44 ^a
Age at surgery, yr, median (IQR)	12.5 (9–16)	11 (7.8–17.3)	13 (9.3–15.8)	0.81 ^b
Age at epilepsy onset, yr, median (IQR)	4 (3–7)	4 (2.5–7.3)	4 (4–6.5)	0.91 ^b
Follow-up period, mo, median (IQR)	24.5 (13–36.5)	23.5 (13.5–42.5)	24.5 (13–29)	0.38 ^b
Resection volume, %, median (IQR) ^c	1.26 (0.90–1.88)	1.45 (1.22–2.12)	1.19 (0.58–1.50)	0.08 ^b
L/R epilepsy side, n	22/6	12/5	10/1	0.35 ^a
T/extra-T lobe, n	7/21	5/12	2/9	0.31 ^a
HD-EEG spike localization, n ^d				0.69 ^a
Clustered	18	10	8	
Scattered	10	7	3	
MEG spike localization, n				0.25 ^a
Clustered	19	10	9	
Scattered	9	7	2	
Dipole–ripple concordance, concordant/total, n (%) ^e				
RZ				
EEG	16/18 (89%)	9/10 (90%)	7/8 (88%)	1 ^a
MEG	14/19 (74%)	9/10 (90%)	5/9 (56%)	0.14 ^a
ROZ				
EEG	17/18 (94%)	9/10 (90%)	8/8 (100%)	1 ^a
MEG	15/18 (79%)	8/9 (89%)	6/9 (67%)	0.58 ^a
Pathology, n				
NL	8	5	3	0.89 ^a
DEV	16	10	6	
ACQ	4	2	2	

^aPearson chi-squared test/Fisher exact test.^bWilcoxon rank sum test; no correction for multiple comparisons was performed.^cResection volume is reported as percentage of brain volume that was removed.^dPatients in whom spike dipoles were “clustered” (ie, formed at least one cluster define as ≥ 5 dipoles within 10mm) versus patients with “scattered” dipoles.^eAnatomical concordance between the preponderant dipole cluster and the lobe with highest presence of RZ (or ROZ) sensors.

ACQ = acquired (ie, stroke, neoplasm, and traumatic brain injury); DEV = malformation of cortical development (ie, focal cortical dysplasia, polymicrogyria, and tuberous sclerosis complex); EEG = electroencephalography; F = female; HD = high-density; IQR = interquartile range; L = center; M = male; MEG = magnetoencephalography; NL = nonlesional; R = right; ROZ = ripple onset zone; RZ = ripple zone; T = temporal.

Fig 4C; $p = 0.074$, 13 vs 18mm). Resection percentages of virtual ROZ ($p = 0.009$) and virtual RZ ($p = 0.03$) estimated via EEG VSs were higher in good than in poor

outcomes (see Fig 4D; $p = 0.009$, $p = 0.03$). Resection percentages of virtual ROZ estimated via MEG VSs was higher in good than in poor outcomes ($p = 0.025$),

TABLE 3. Characteristics of Ripples and Their Spatiotemporal Propagation on Intracranial and Virtual Implantation

Characteristic	Modality			<i>p</i>		
	icEEG	EEG VSs	MEG VSs	EEG vs icEEG	MEG vs icEEG	EEG vs MEG
Occurrence rate, ripples/min ^a	3.4 (2.7–6)	0.9 (0.6–1.6)	0.4 (0.2–0.8)	<0.001	<0.001	<0.001
Ripple frequency, Hz ^b	90 (89–93)	94 (92–99)	100 (95–112)	0.002	<0.001	0.017
Propagation sequences per min	15 (8.7–27.8)	5.4 (3.8–10)	2.4 (1–5.7)	<0.001	<0.001	<0.001
Temporal extent, ms ^c	86 (64–101)	27 (16–47)	22 (17–30)	<0.001	<0.001	0.17
Spatial extent, mm ^d	32 (26–38)	41 (33–64)	36 (25–52)	<0.001	0.09	<0.001
Spatial extent, sensors, n	5 (4–6)	6 (5–7)	5 (4–7)	0.02	0.21	0.04
Latency of ripples from onset, ms	62 (44–73)	29 (26–35)	27 (23–37)	<0.001	<0.001	0.36
Latency between ripples, ms	32 (25–40)	7 (5–11)	7 (6–11)	<0.001	<0.001	0.75
Onset sensors per propagation, n	1 (1–2)	4 (4–9)	4 (3–7)	<0.001	<0.001	0.003
Onset sensors per propagation, %	35% (32–41)	70% (59–78)	69% (62–76)	<0.001	<0.001	0.53

Numbers in parentheses represent interquartile range.

^aAverage occurrence rate (ripples/min) across all sensors showing ripples.

^bAverage peak frequency of each ripple, computed as the frequency showing the maximum power within the ripple frequency range.

^cTemporal interval between the onset of the first and last ripple of a propagation sequence.

^dMaximum distance between sensors within a propagation sequence.

EEG = electroencephalography; icEEG = intracranial EEG; MEG = magnetoencephalography; VS = virtual sensor.

whereas this was not the case for the virtual RZ ($p = 0.12$). D_{RES} of both virtual ROZ and virtual RZ estimated via MEG VSs did not differ between outcome groups ($p = 0.0887$, $p = 0.082$).

Regarding spikes, the resection percentage, as well as D_{RES} , did not differ between good and poor outcomes (see Fig 4D, E) for HD-EEG ($p = 0.72$, $p = 0.42$) and MEG ($p = 0.83$, $p = 0.96$). Additionally, in good outcome patients (proof of successful resection), both virtual RZ and virtual ROZ were closer to resection compared to spike localization for both HD-EEG ($p = 0.0016$, $p < 0.001$) and MEG ($p = 0.003$, $p = 0.001$). Table 4 reports distances and overlap between spike sources and ripple zones.

Finally, virtual RZ presented a D_{SOZ} of 14 and 16mm for MEG and HD-EEG, respectively ($p = 0.01$), and overlap with SOZ of 33% (19–45%) and 29% (13–40%, $p = 0.0095$). Virtual ROZ showed a D_{SOZ} of 13 and 14mm for MEG and HD-EEG, respectively ($p = 0.68$), and overlap of 33% (15–49%) and 30% (15–50%, $p = 0.64$).

Outcome Prediction

At the individual patient level, resecting the virtual ROZ predicted good outcome (see Table 4), with PPV of 91%, NPV of 59%, and accuracy of 71% when estimated via

EEG VSs ($p = 0.016$), and PPV of 83%, NPV of 60%, and accuracy of 70% when estimated via MEG VSs ($p = 0.047$). In contrast, no association was found for the virtual RZ estimated via EEG VSs ($p = 0.125$), whereas a weak association was found with MEG VSs ($p = 0.054$; Table 4).

When looking at spikes, resecting most of dipoles (resection percentage > 50%) did not predict outcome for HD-EEG ($p \sim 1$) or MEG ($p = 0.67$).

Discussion

We present for the first time the noninvasive mapping of interictal ripple propagation in children with MRE using electric and magnetic source imaging. We previously showed ripple spatiotemporal propagation on icEEG, demonstrating the prognostic value of its onset generator (ROZ) for pediatric epilepsy surgery compared to areas of spread.²¹ This earlier study, followed by Otárola et al,²² demonstrated that interictal HFOs are not isolated events on icEEG, but pathophysiological activity organized in networks. Here, we present evidence that this epileptogenic phenomenon of ripple propagation can be captured noninvasively through a virtual implantation (reconstructed using HD-EEG or MEG) and show its value as an outcome predictor in children with MRE. Our

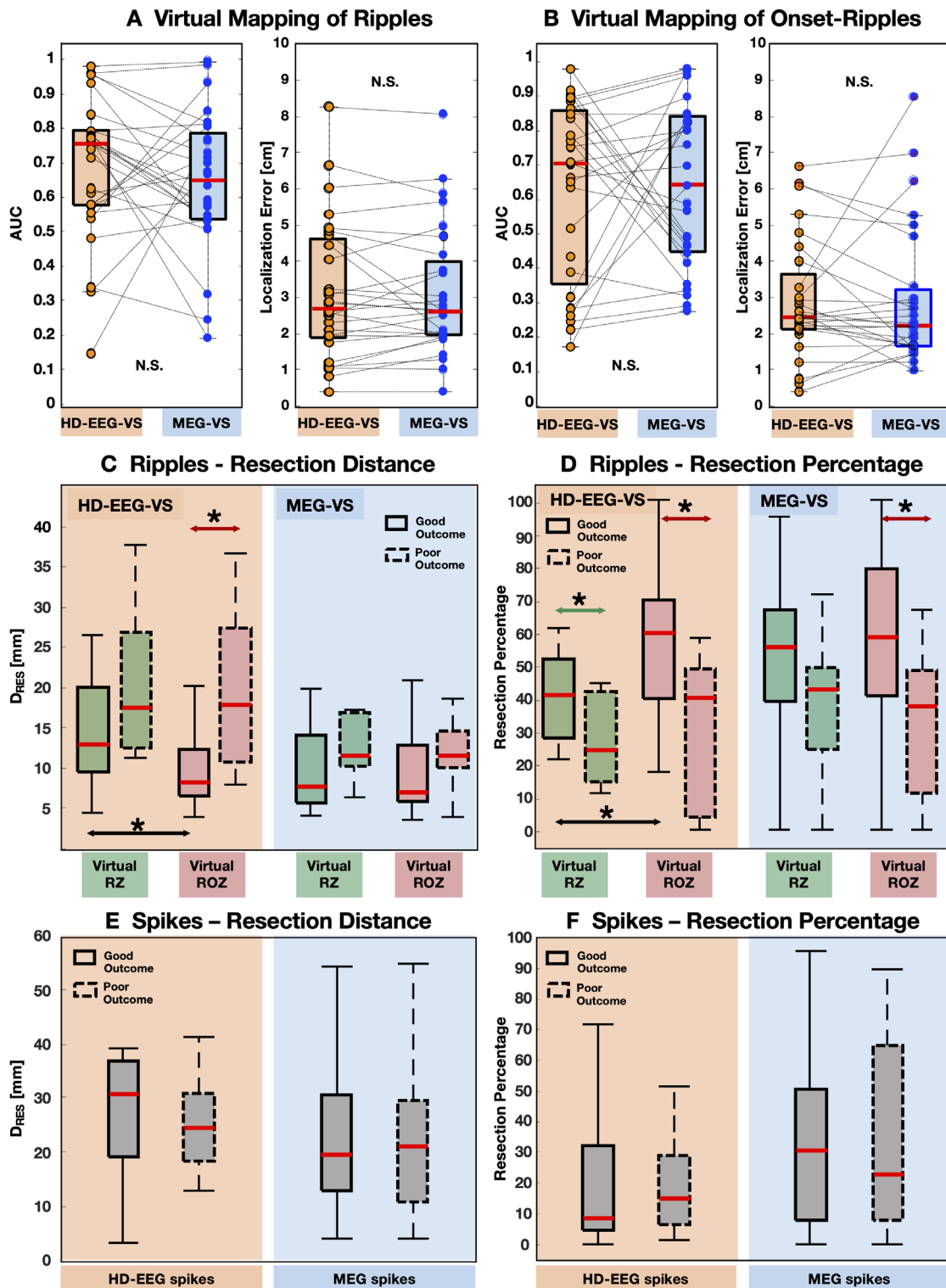


FIGURE 4: Results from validation of virtual zones versus invasive electroencephalography (EEG) and resection. Significant differences ($p < 0.05$) are marked with asterisks. (A, B) Validation of the virtual mapping of ripples (A) and onset ripples (B) against the benchmark given by intracranial EEG (icEEG). Each scenario shows the boxplots of the (1) area under the curve (AUC) obtained from each patient using high-density (HD)-EEG virtual sensors (VSs; orange) and magnetoencephalography (MEG) VSs (blue); and (2) median distance of VSs from intracranial ripple zone (RZ) or intracranial ripple onset zone (ROZ; D_{icEEG}) in centimeters. Differences between modalities were not statistically significant (N.S.; $p > 0.05$). No difference was observed when we differentiated D_{icEEG} for the icEEG contacts in the gray and white matter ($p > 0.1$). (C, D) Boxplots of the distance from resection (D_{RES} ; C) and resection percentage (D) for virtual RZ (in green) and virtual ROZ (in red) in good versus poor outcome (solid vs dashed box) patients. Each scenario shows boxplots for both HD-EEG VSs and MEG VSs. (E, F) Boxplots of D_{RES} (E) and resection percentage (F) for interictal spikes in good versus poor outcome (solid vs dashed box) patients. Each scenario shows boxplots for both HD-EEG VSs and MEG VSs.

TABLE 4. Predictive Value of Removing the Virtual Zones

Modality	Ripple Zone				Ripple Onset Zone			
	EEG VSs		MEG VSs		EEG VSs		MEG VSs	
Virtual rate threshold	0.25		0.5		0.55		0.35	
Residual, $\geq 50\%$ not resected ^a	No	Yes	No	Yes	No	Yes	No	Yes
Outcome								
Good, seizure-free	5	12	10	7	10	7	10	6
Poor, seizure recurrence	0	11	2	9	1	10	2	9
Total	5	23	12	16	11	17	12	15
PPV	100%		83%		91%		83%	
NPV	48%		56%		59%		60%	
Accuracy	57%		68%		71%		70%	
<i>Phi</i>	0.38		0.40		0.50		0.44	
Fisher exact test	0.125		0.054		0.016 ^b		0.047 ^b	
Comparison of ripple and spike localization								
Distance of ripple VSs from spikes, mm ^c	23 (18–29)		17 (14–25)		15 (12–29)		16 (12–27)	
Distance of spikes from ripple VSs, mm ^d	24 (19–30)		30 (25–41)		27 (18–35)		29 (20–41)	
Overlap with spikes ^e	14% (3–22%)		17% (4–36%)		24% (0–40%)		14% (0–38%)	

Numbers in parentheses represent interquartile range.

^aA zone was regarded as “residual” after surgery if the resection percentage was $< 50\%$.

^bSignificant *p* value (> 0.05); Fisher exact test.

^cDistance of the VSs (center) from the closest spike source (dipole).

^dDistance of the spike sources from the closest VS (center).

^eOverlap was defined as the percentage of VSs with a distance from the closest dipole < 10 mm.

EEG = electroencephalography; MEG = magnetoencephalography; NPV = negative predictive value; *Phi* = *Phi* coefficient of association; PPV = positive predictive value; VS = virtual sensor.

data indicate that ripple propagation, as captured by VSs, reflects the hierarchical epileptogenic organization seen on icEEG²¹; mapping the ripple onset generator (virtual ROZ) estimates the EZ better than mapping all ripple generators independently from propagation (virtual RZ). This derives from our main findings: (1) EEG VSs and MEG VSs, placed over specific brain areas, can capture ripples and their propagation onset; (2) areas generating ripples (RZ) and initiating their propagation (ROZ) are localized via VSs with an accuracy that is similar between HD-EEG and MEG; and (3) resecting the virtual ROZ, but not virtual RZ or spike sources, predicts good outcome (seizure freedom) in pediatric epilepsy surgery.

Ripple Propagation Is Captured Noninvasively by VSs

The concept of propagation in epilepsy is typically used when interpreting seizure semiology or ictal recordings.

For scalp EEG or MEG, the concept of onset is generally applied when interpreting ictal activity (SOZ) but also interictal spikes if propagation is seen.^{39–41} Only recently, interictal propagation was also reported for ripples on icEEG.^{21,22} Here, we add to that evidence, revealing this phenomenon on HD-EEG or MEG VSs as well; we found that interictal ripples define distinct spatiotemporal sequences across multiple (4–7) neighboring VSs (see Fig 2) as observed on invasive recordings, although with lower rates. Ripple onset areas on VSs showed an overall spatial concordance with icEEG (~ 2 cm), whereas, in terms of duration, propagations appear shorter on VSs than icEEG (see Table 3), suggesting that VSs may miss some later spread, which is seen instead on icEEG. Given the lack of association between spread ripples and EZ demonstrated on icEEG,²¹ the absence of such activity on VSs does not hamper presurgical clinical relevance. Furthermore, ripple

propagation on VSs covers slightly larger distance than on icEEG (36–41 vs 32mm) and larger areas of onset (4 VSs vs 1 icEEG contact); this possibly reflects the lower spatial resolution of noninvasive techniques and thus lower accuracy in estimating the extent of the generators.

Our findings provide the first robust evidence that ripple propagation can be captured using virtual, rather than invasive, sensors and stimulate further methodological studies to develop automated methods to investigate ripple propagation via full-coverage VSs. Although our VSs were placed to replicate icEEG retrospectively, our findings suggest that they can be eventually placed at desired locations in a prospective way.

HD-EEG and MEG VSs Map Ripples and Their Onset with Similar Accuracy

We quantified the ability of VSs to map ripples (RZ) and their propagation onset (ROZ) with respect to icEEG. We observed no difference between HD-EEG and MEG performance, both showing $D_{icEEG} < 3$ cm (RZ ~ 26 mm, ROZ ~ 23 mm). AUCs < 0.5 , observed in some patients, denote spatial discrepancy between virtual and icEEG ripple rates; this may be explained by the fact that HD-EEG/MEG and icEEG recordings were not simultaneous and thus may have captured different ripple sources due to their variability across time.^{42,43}

We can assume that VSs over specific brain areas grant a ripple localization within the same (or most proximal) gyrus (~ 2 – 3 cm) that is indicated by an invasive implantation covering the same areas. Reconstructing high-frequency activation noninvasively with 2 to 3cm accuracy could impact surgical planning, enabling the clinical team to optimize implantation options. Nonetheless, when the EZ is adjacent to eloquent areas, more accurate biomarkers are required. Overall, our data demonstrate spatial consistency between ripples on VSs and icEEG, suggesting they are expressions of the same underlying phenomenon^{15,44} and expanding this notion to their propagation onset.

Regarding the comparison with spikes, although the vast majority of the virtual ripple zones did not overlap in a strict sense (< 10 mm apart) with spike sources, they seem to be just adjacent (15–23mm; see Table 4); preponderant spike clusters presented lobar concordance with ripples in most cases (see Table 2).

Virtual Mapping of Onset Ripples Estimates the EZ Better Than All Ripples or Spikes

In the presurgical context, it is key to evaluate an epilepsy biomarker with respect to the ground truth of good outcome after resection. We found that identifying areas of

ripple onset (virtual ROZ) reflects epileptogenicity better than identifying indistinctively all VSs showing ripples (virtual RZ) regardless of any propagation characteristics. For the virtual RZ, we found no differences in its proximity to resection between outcomes. In contrast, virtual ROZ was closer to resection in good than poor outcome patients when estimated via EEG VSs; in addition, in good outcomes, it was closer to resection (8mm) than the virtual RZ (13mm). For MEG VSs, the resection percentage of the virtual ROZ (but not virtual RZ) was higher in good (59%) than in poor outcome patients (38%). These noninvasive findings corroborate previous icEEG data²¹ that emphasized the pathological nature of onset ripples as opposed to other ripples (spread or isolated), which seem more likely to reflect physiological mechanisms. Additionally, spike localization with HD-EEG or MEG presented lower performance than virtual RZ or virtual ROZ: (1) resection percentage and D_{RES} did not differ between outcomes; and (2) in good outcomes, virtual RZ and virtual ROZ were closer to resection than spikes (dipoles). Because dipoles do not estimate the spike spatial extent, we acknowledge that our reported distances from resection may represent an overestimate and warrant further investigations with distributed source modeling (DSM).⁴⁵ However, because DSM on spikes was recently reported to provide an average improvement of only ~ 1 mm (compared to dipoles) in adults,⁴⁶ we speculate that this may not affect significantly our main findings.

Resection of ROZ, but Not Entire RZ or Spikes, Predicts Good Outcome

To assess clinical utility in terms of individualized care, we investigated the predictive value of resecting virtually defined zones. Removing most of the virtual ROZ predicted outcome with PPV and NPV of 83–91% and 59–60%, suggesting the prognostic value of targeting this zone during surgery. In contrast, targeting the virtual RZ, that is, regions generating any type of ripple, presented lower predictive values. Additionally, spike localization provided complementary information to the ROZ or RZ (given their low overlap) and did not carry prognostic value. We showed the superiority of mapping ripple onset compared to indistinctively locating all the sites showing ripples on VSs or localizing spikes in the traditional sense. This adds to previous efforts aimed at recognizing the most pathological ripples, which so far was mostly performed through their relationship with spikes^{15,19} or morphological features.^{47–49} Our findings reveal that the spatiotemporal characterization of ripples enhances their interpretation on scalp HD-EEG and MEG; evaluating whether it is possible to resect the areas initiating the

propagation on VSs provides an additional noninvasive estimate of the EZ, especially when invasive monitoring cannot be easily planned.

Although the association between outcome and virtual RZ resection did not reach significance, it showed the same predictive trend for MEG VSs ($p = 0.054$; see Table 4) and EEG VSs (see Fig 4D). This suggests that ripples on HD-EEG/MEG are less undermined by physiological counterparts than on icEEG⁵⁰ (which is more sensitive to low amplitude and spread activity); this also explains low ripple rates typically observed in noninvasive studies.^{14,15,25}

Limitations

Applicability of our approach is limited to the eligible patients; we excluded 1-stage resections and children who were not referred for HD-EEG/MEG. Generalizability to spike-negative patients and reproducibility across HD-EEG/MEG sessions need further investigation. We constructed VSs at the icEEG locations to allow direct comparison with icEEG (the technique of choice to record ripples and propagation); future studies are warranted to assess the potential of whole-brain VSs. Although automated ripple detection cannot fully exclude artifacts, our detector is particularly robust, because it rejects events showing elongated time–frequency blobs. Our analysis excluded fast ripples, because there is limited evidence of their presence on scalp EEG or MEG, and we had a 600Hz sampling rate in several recordings. In addition, some of the observed ripples may be physiological (eg, low-amplitude ripples in Fig 2); further MEG/HD-EEG investigations of ripples overlapping on spikes are warranted. Finally, the use of HD-EEG systems with a higher number of channels (eg, 256)⁴⁵ is likely to improve the localization accuracy of ripples and allow fairer comparisons with MEG.

Conclusions

We revealed the noninvasive mapping of interictal ripple propagation in children with MRE, using HD-EEG and MEG, and demonstrated its prognostic value. Performing a noninvasive implantation of VSs over specific brain areas allows mapping the ripple propagation onset (ROZ), an area that yields prognostic value as an EZ biomarker in epilepsy surgery. Removing areas of ripple onset, as defined by the virtual implantation, predicts good outcome better than the entire area generating ripples or spikes. This noninvasive mapping may augment surgical planning, potentially improving outcomes of pediatric epilepsy surgery.

Acknowledgments

This work was supported by the NIH National Institute of Neurological Disorders and Stroke (7R01NS104116, Principal Investigator (PI): Christos Papadelis; and 7R21NS101373, PIs: Christos Papadelis and Steve M. Stuffelbeam).

Author Contributions

E.T, S.M.S., P.L.P., and C.P. contributed to the conception and design of the study. E.T, M.A.G.M., G.N., J.R.M., P.E.G., and C.P. contributed to the acquisition and analysis of data. E.T., M.A.G.M., P.L.P., and C.P. contributed to drafting a significant portion of the manuscript and figures.

Potential Conflicts of Interest

Nothing to report.

References

- Rosenow F, Lüders H. Presurgical evaluation of epilepsy. *Brain* 2001; 124:1683–1700.
- Frauscher B. Localizing the epileptogenic zone. *Curr Opin Neurol* 2020;33:1–9.
- Zijlmans M, Zweiphenning W, van Klink N. Changing concepts in presurgical assessment for epilepsy surgery. *Nat Rev Neurol* 2019; 15:594–606.
- Vakharia VN, Duncan JS, Witt JA, et al. Getting the best outcomes from epilepsy surgery. *Ann Neurol* 2018;83:676–690.
- Zijlmans M, Jiruska P, Zelmann R, et al. High frequency oscillations as a new biomarker in epilepsy. *Ann Neurol* 2012;71:169–178.
- Jacobs J, Zijlmans M, Zelmann R, et al. High-frequency electroencephalographic oscillations correlate with outcome of epilepsy surgery. *Ann Neurol* 2010;67:209–220.
- Thomschewski A, Hincapié AS, Frauscher B. Localization of the epileptogenic zone using high frequency oscillations. *Front Neurol* 2019;10:94.
- Malinowska U, Bergey GK, Harezlak J, Jouny CC. Identification of seizure onset zone and preictal state based on characteristics of high frequency oscillations. *Clin Neurophysiol* 2015;126:1505–1513.
- Frauscher B, Bartolomei F, Kobayashi K, et al. High-frequency oscillations: the state of clinical research. *Epilepsia* 2017;58:1316–1329.
- Zijlmans M, Worrell GA, Dumpelmann M, et al. How to record high-frequency oscillations in epilepsy: a practical guideline. *Epilepsia* 2017;58:1305–1315.
- Tamilia E, Madsen JR, Grant PE, et al. Current and emerging potential of magnetoencephalography in the detection and localization of high-frequency oscillations in epilepsy. *Front Neurol* 2017;8:1–28.
- Akiyama T, McCoy B, Go CY, et al. Focal resection of fast ripples on extraoperative intracranial EEG improves seizure outcome in pediatric epilepsy. *Epilepsia* 2011;52:1802–1811.
- Schevon CA, Trevelyan AJ, Schroeder CE, et al. Spatial characterization of interictal high frequency oscillations in epileptic neocortex. *Brain* 2009;132:3047–3059.
- von Ellenrieder N, Pellegrino G, Hedrich T, et al. Detection and magnetic source imaging of fast oscillations (40–160 Hz) recorded with

- magnetoencephalography in focal epilepsy patients. *Brain Topogr* 2016;29:218–231.
15. Tamilia E, Dirodi M, Alhilani M, et al. Scalp ripples as prognostic biomarkers of epileptogenicity in pediatric surgery. *Ann Clin Transl Neurol* 2020;7:329–342.
 16. Andrade-Valenca LP, Dubeau F, Mari F, et al. Interictal scalp fast oscillations as a marker of the seizure onset zone. *Neurology* 2011; 77:524–531.
 17. Papadelis C, Tamilia E, Stufflebeam S, et al. Interictal high frequency oscillations detected with simultaneous magnetoencephalography and electroencephalography as biomarker of pediatric epilepsy. *J Vis Exp* 2016;118:54883.
 18. Melani F, Zemann R, Dubeau F, Gotman J. Occurrence of scalp-fast oscillations among patients with different spiking rate and their role as epileptogenicity marker. *Epilepsy Res* 2015;106:345–356.
 19. Wang S, Wang IZ, Bulacio JC, et al. Ripple classification helps to localize the seizure-onset zone in neocortical epilepsy. *Epilepsia* 2013;54:370–376.
 20. Urrestarazu E, Jirsch JD, LeVan P, et al. High-frequency intracerebral EEG activity (100–500 Hz) following interictal spikes. *Epilepsia* 2006; 47:1465–1476.
 21. Tamilia E, Park EH, Percivati S, et al. Surgical resection of ripple onset predicts outcome in pediatric epilepsy. *Ann Neurol* 2018;84: 331–346.
 22. Otárola KAG, von Ellenrieder N, Cuello-Oderiz C, et al. High-frequency oscillation networks and surgical outcome in adult focal epilepsy. *Ann Neurol* 2019;85:485–494.
 23. Nissen IA, Stam CJ, Reijneveld JC, et al. Identifying the epileptogenic zone in interictal resting-state MEG source-space networks. *Epilepsia* 2017;58:137–148.
 24. van Klink N, van Rosmalen F, Nenonen J, et al. Automatic detection and visualisation of MEG ripple oscillations in epilepsy. *Neuroimage Clin* 2017;15:689–701.
 25. van Klink N, Mooij A, Huiskamp G, et al. Simultaneous MEG and EEG to detect ripples in people with focal epilepsy. *Clin Neurophysiol* 2019;130:1175–1183.
 26. van Klink N, Hillebrand A, Zijlmans M. Identification of epileptic high frequency oscillations in the time domain by using MEG beamformer-based virtual sensors. *Clin Neurophysiol* 2016;127: 197–208.
 27. Nissen IA, van Klink N, Zijlmans M, et al. Brain areas with epileptic high frequency oscillations are functionally isolated in MEG virtual electrode networks. *Clin Neurophysiol* 2016;127:2581–2591.
 28. Migliorelli C, Alonso JF, Romero S, et al. Automated detection of epileptic ripples in MEG using beamformer-based virtual sensors. *J Neural Eng* 2017;14:046013.
 29. Tamilia E, Alhilani M, Tanaka N, et al. Assessing the localization accuracy and clinical utility of electric and magnetic source imaging in children with epilepsy. *Clin Neurophysiol* 2019;130:491–504.
 30. Tadel F, Baillet S, Mosher JC, et al. Brainstorm: a user-friendly application for MEG/EEG analysis. *Comput Intell Neurosci* 2011;2011: 879716.
 31. Blenkmann AO, Phillips HN, Princhin JP, et al. iElectrodes: a comprehensive open-source toolbox for depth and subdural grid electrode localization. *Front Neuroinform* 2017;11:14.
 32. Dale AM, Fischl B, Sereno MI. Cortical surface-based analysis. *Neuroimage* 1999;9:179–194.
 33. Gramfort A, Papadopoulos T, Olivi E, Clerc M. OpenMEEG: opensource software for quasistatic bioelectromagnetics. *Biomed Eng Online* 2010;9:45.
 34. Alhilani M, Tamilia E, Ricci L, et al. Ictal and interictal source imaging on intracranial EEG predicts epilepsy surgery outcome in children with focal cortical dysplasia. *Clin Neurophysiol* 2020;131:734–743.
 35. Ono M, Kubik S, Abernathy C. *Atlas of the cerebral sulci*. New York, NY: Thieme Medical Publishers, 1990.
 36. Kim D, Joo EY, Seo DW, et al. Accuracy of MEG in localizing irritative zone and seizure onset zone: quantitative comparison between MEG and intracranial EEG. *Epilepsy Res* 2016;127:291–301.
 37. Diekmann V, Decker W, Jürgens R, et al. Localisation of epileptic foci with electric, magnetic and combined electromagnetic models. *Electroencephalogr Clin Neurophysiol* 1998;106:297–313.
 38. Almubarak S, Alexopoulos A, Von-Podewils F, et al. The correlation of magnetoencephalography to intracranial EEG in localizing the epileptogenic zone: a study of the surgical resection outcome. *Epilepsy Res* 2014;108:1581–1590.
 39. Westmijse I, Ossenblok P, Gunning B, Van Luitelaar G. Onset and propagation of spike and slow wave discharges in human absence epilepsy: a MEG study. *Epilepsia* 2009;50:2538–2548.
 40. Tanaka N, Grant PE, Suzuki N, et al. Multimodal imaging of spike propagation: a technical case report. *Am J Neuroradiol* 2012;33: 82–84.
 41. Tanaka N, Hämäläinen M, Ahlfors SP, et al. Propagation of epileptic spikes reconstructed from spatiotemporal magnetoencephalographic and electroencephalographic source analysis. *Neuroimage* 2010;50: 217–222.
 42. Conrad EC, Tomlinson SB, Wong JN, et al. Spatial distribution of interictal spikes fluctuates over time and localizes seizure onset. *Brain* 2020;143:554–569.
 43. Gliske SV, Irwin ZT, Chestek C, et al. Variability in the location of high frequency oscillations during prolonged intracranial EEG recordings. *Nat Commun* 2018;9:2155.
 44. Dirodi M, Tamilia E, Grant PE, et al. Noninvasive localization of high-frequency oscillations in children with epilepsy: validation against intracranial gold-standard. *Annu Int Conf IEEE Eng Med Biol Soc* 2019;2019:1555–1558.
 45. Avigdor T, Abdallah C, von Ellenrieder N, et al. Fast oscillations localize the epileptogenic zone: an electrical source imaging study using high-density electroencephalography. *Clin Neurophysiol* 2021; 132:568–580.
 46. Pellegrino G, Hedrich T, Chowdhury RA, et al. Clinical yield of magnetoencephalography distributed source imaging in epilepsy: a comparison with equivalent current dipole method. *Hum Brain Mapp* 2017;39:218–231.
 47. Matsumoto A, Brinkmann BH, Stead SM, et al. Pathological and physiological high-frequency oscillations in focal human epilepsy. *J Neurophysiol* 2013;110:1958–1964.
 48. Cimbalnik J, Brinkmann B, Kremen V, et al. Physiological and pathological high frequency oscillations in focal epilepsy. *Ann Clin Transl Neurol* 2018;5:1062–1076.
 49. Blanco JA, Stead M, Krieger A, et al. Data mining neocortical high-frequency oscillations in epilepsy and controls. *Brain* 2011;134: 2948–2959.
 50. Fauscher B, von Ellenrieder N, Zemann R, et al. High-frequency oscillations in the normal human brain. *Ann Neurol* 2018;84: 374–385.